

# Reassessment of Probabilistic Seismic Hazard in the Marmara Region

by Erol Kalkan, Polat Gülkan, Nazan Yılmaz, and Mehmet Çelebi

**Abstract** In 1999, the eastern coastline of the Marmara region (Turkey) witnessed increased seismic activity on the North Anatolian fault (NAF) system with two damaging earthquakes ( $M$  7.4 Kocaeli and  $M$  7.2 Düzce) that occurred almost three months apart. These events have reduced stress on the western segment of the NAF where it continues under the Marmara Sea. The undersea fault segments have been recently explored using bathymetric and reflection surveys. These recent findings helped scientists to understand the seismotectonic environment of the Marmara basin, which has remained a perplexing tectonic domain. On the basis of collected new data, seismic hazard of the Marmara region is reassessed using a probabilistic approach. Two different earthquake source models: (1) the smoothed-gridded seismicity model and (2) fault model and alternate magnitude-frequency relations, Gutenberg–Richter and characteristic, were used with local and imported ground-motion-prediction equations. Regional exposure is computed and quantified on a set of hazard maps that provide peak horizontal ground acceleration (PGA) and spectral acceleration at 0.2 and 1.0 sec on uniform firm-rock site condition (760 m/sec average shear wave velocity in the upper 30 m). These acceleration levels were computed for ground motions having 2% and 10% probabilities of exceedance in 50 yr, corresponding to return periods of about 2475 and 475 yr, respectively. The maximum PGA computed (at rock site) is  $1.5g$  along the fault segments of the NAF zone extending into the Marmara Sea. The new maps generally show 10% to 15% increase for PGA, 0.2 and 1.0 sec spectral acceleration values across much of Marmara compared to previous regional hazard maps. Hazard curves and smooth design spectra for three site conditions: rock, soil, and soft-soil are provided for the Istanbul metropolitan area as possible tools in future risk estimates.

## Introduction

The Marmara region houses one-third of Turkey's population and is one of the most tectonically active regions in Eurasia. In the last century, this region (Fig. 1) experienced unusual seismic activity with nine strong events having  $M \geq 7.0$  ( $M$  = moment magnitude). In 1999, two destructive earthquakes (Kocaeli and Düzce) occurred in the eastern part of the Marmara region on the North Anatolian fault (NAF) system. This strike-slip fault system cuts across northern Turkey for more than 1200 km and accommodates  $\sim 25$  mm/yr right-lateral slip between the Anatolian and Eurasian plates (Straub *et al.* 1997; McClusky *et al.* 2000). Since 1939, the NAF system has produced nine large earthquakes in a consistently westward-propagating sequence (Fig. 2); the only exception is the most recent large earthquake (Düzce) that occurred east of the second most-recent earthquake (Kocaeli). This pattern of earthquake propagation was recognized long ago (Ketin, 1969; Ambraseys, 1970; Barka, 1992; Stein *et al.*, 1997).

The Kocaeli earthquake ( $M$  7.4) is the most recent event that occurred on the south of the eastern border of the

Istanbul province, which is located in the heart of the Marmara region. Today, this most-populated city in Europe is under threat of much publicized forecasted earthquakes. Two fault systems located south and southeast of Istanbul (the Yalova fault segment and the northern boundary fault) have the potential to rupture (Parsons *et al.*, 2000; Hubert-Ferrari *et al.*, 2000). Based on a renewal model, the probability of occurrence of  $M$  7.0 and greater earthquakes in the Marmara region that could directly influence the Istanbul metropolitan area was computed as  $44 \pm 18\%$  in the next 30 yr (Parsons, 2004). As implied by the level of seismic risk, critical assessment of the regional seismic hazard is of paramount importance to facilitate and support a wide range of earthquake engineering applications.

The current regulatory seismic zoning map of Turkey, including the Marmara region, was developed using a Bayesian estimation based on then available earthquake catalog and ground-motion-prediction equations (GMPEs) originally developed from western U.S. ground motion data (Gülkan *et al.*, 1993). This choice was dictated by the paucity of

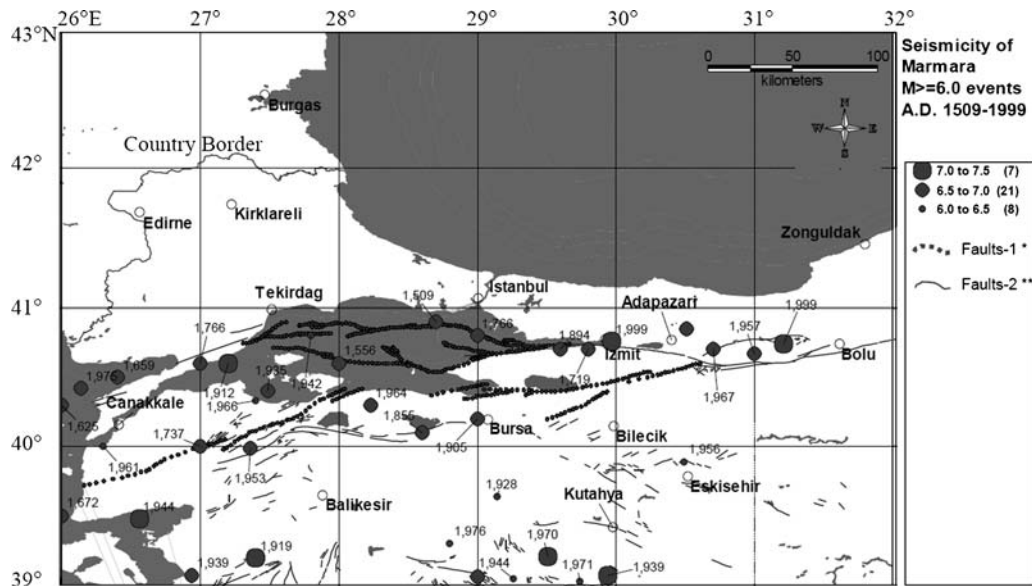


**Figure 1.** Seismicity of the Marmara region based on  $M \geq 6.0$  events (A.D. 1509–1999). The numbers of earthquakes are given in parentheses. Faults-1\* type faults were recently visualized using bathymetric images and seismic reflection surveys (Le Pichon *et al.*, 2001; Armijo *et al.*, 2002; Le Pichon *et al.*, 2003; Armijo *et al.*, 2005) and Faults-2\*\* type faults are previously known faults (Saroglu *et al.*, 1992); see Table 1 for epicenter coordinates, magnitudes, and depths of earthquakes.

strong-motion records in the country at the time. In the past 15 yr, a number of strong-motion records have been recorded in Turkey, mainly from the 1999 Kocaeli  $M$  7.4 and Duzce  $M$  7.2 events, and hence, prompted development of national GMPEs (e.g., Gülkan and Kalkan, 2002; Kalkan and Gülkan, 2004; Ulusay *et al.*, 2004). In addition, tracing of new fault segments beneath the Marmara Sea has helped better understanding of the seismotectonic environment of the Marmara basin (Le Pichon *et al.*, 2001; Armijo *et al.*, 2002; Le Pichon *et al.*, 2003; Armijo *et al.*, 2005).

Seismic hazard of the Marmara region has been studied previously (Atakan *et al.*, 2002; Erdik *et al.*, 2004). These studies are based on broadly described fault segments under the Marmara Sea and nonindigenous GMPEs from the 1990s. In our study, the regional seismic hazard is reassessed by considering detailed submarine faults and using the latest

generation of GMPEs. The next generation of attenuation (NGA) relations (Boore and Atkinson, 2008; Campbell and Bozorgnia, 2008; Chiou and Youngs, 2008) are used in addition to the GMPE of Kalkan and Gülkan, developed based on data from shallow crustal tectonic environment of Turkey. The weight assigned to the local GMPE is set equal to total weight of the NGA relations.

In computing the probabilistic seismic hazard, we include two different earthquake source models: (1) smoothed-gridded seismicity model and (2) fault model, similar to those used in the development of the 2008 USGS National Seismic Hazard Maps (Petersen *et al.* 2008). The first model assumes that historical large earthquakes have in general taken place in locations where epicenters of smaller earthquakes have accumulated (Kafka and Walcott, 1998; Kafka, 2002). This model is based on the earthquake catalog and characterizes

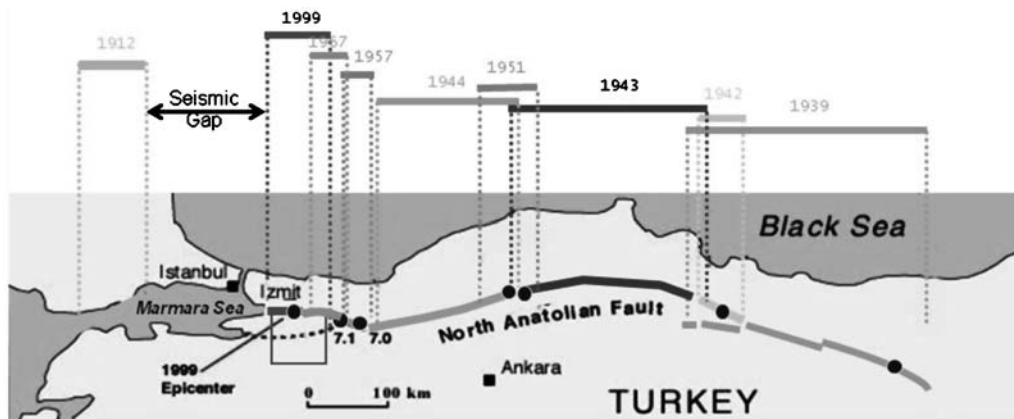


**Figure 2.** Westward propagating sequence of earthquakes on the North Anatolian fault system since 1939.

the hazard from earthquakes between  $M$  4.0 and 6.5. The faults contribute to the hazard for earthquakes larger than  $M$  6.5. The hazard calculation is the sum of the smoothed-gridded seismicity model (for  $M \leq 6.5$ ) and the fault model (for  $M \leq 6.5$ ).

Seismic hazard of Marmara is computed and projected on a set of hazard maps. These hazard maps show the PGA and spectral accelerations (SA) at 0.2 and 1.0 sec on uniform firm-rock site condition ( $V_{S30} = 760$  m/sec). In the interest of completeness, site amplification maps are also provided to estimate the ground motion at stiff-soil ( $V_{S30} = 360$  m/sec) and soft-soil ( $V_{S30} = 180$  m/sec) sites. These acceleration levels were computed for 2% and 10% probabilities of exceedance in 50 yr corresponding to return periods of about 2475 and 475 yr, respectively. The seismic hazard exposures in the vicinity of Istanbul metropolitan area are also examined, and a series of hazard curves and smooth design spectra for three site categories are provided.

### Regional Tectonic Setting

For the purpose of this study, the Marmara region is defined as the rectangular area bounded by latitudes  $39^{\circ}$ – $43^{\circ}$  N and longitudes of  $26^{\circ}$ – $32^{\circ}$  E. The area is one of the most tectonically active regions of Turkey as evidenced by the number of large earthquakes ( $M \geq 6.0$ ) that have occurred between 1509 and 1999 (Fig. 1). Many of these events were  $M \geq 7.0$  and generated on or in proximity of the NAF system. Moderate to large earthquakes with  $M \geq 6.0$  have also occurred on fault segments situated well away from the NAF. Figure 3 depicts the distribution of all distinct events with  $M \geq 4.0$  that occurred in the period 1901–2004. The figure also shows the breakdown of the number of earthquakes within each magnitude interval.

The Marmara region has a complex and heterogeneous fault system as shown in Figure 4. The 1200 km long NAF fault system extends from the east of the region toward the Bay of Izmit. In the east at the junction of the Marmara Sea, the NAF system is controlled by right-lateral strike-slip faults, while the plate boundary changes into a transtensional system that has opened a deep-basin below the Marmara Sea (Okay *et al.*, 2000). There is no evidence of a single, continuous, purely strike-slip fault under the Marmara Sea, but there is a complex segmented fault system with large normal components. This fault system has been identified from seismic reflection surveys (Smith *et al.*, 1995; Parke *et al.*, 1999). In the past a series of strong earthquakes has ruptured the NAF zone in this region. Kocaeli and Düzce were the latest events in a westward-propagating earthquake sequence that began with the  $M$  7.9 Erzincan earthquake in 1939 on this fault system. This progression has since generated nine  $M \geq 7$  earthquakes. When the 1912 event that occurred in the west of the Marmara Sea is taken into account, a seismic gap that has not ruptured for more than 200 yr is identified (Fig. 2). This crosses close to the northern shoreline of the Marmara Sea (Barka, 1992; Stein *et al.*, 1997). This seismic gap is around 150–160 km long and possesses the potential to generate an  $M \geq 7$  earthquake (Hubert-Ferrari *et al.*, 2000). Coulomb stress calculations indicate that shear stress increased in the aftermath of the 1999 Kocaeli earthquake on the fault segments below the sea, which may indicate their likely impact on the rupture potential (Parsons *et al.*, 2000).

The measured slip vectors in the Anatolian plate with respect to the stable Eurasian plate exhibit a generally anticlockwise rotation and an increase in total displacement toward the west caused by the increasing westward pull of the Hellenic subduction system located southwest of Turkey

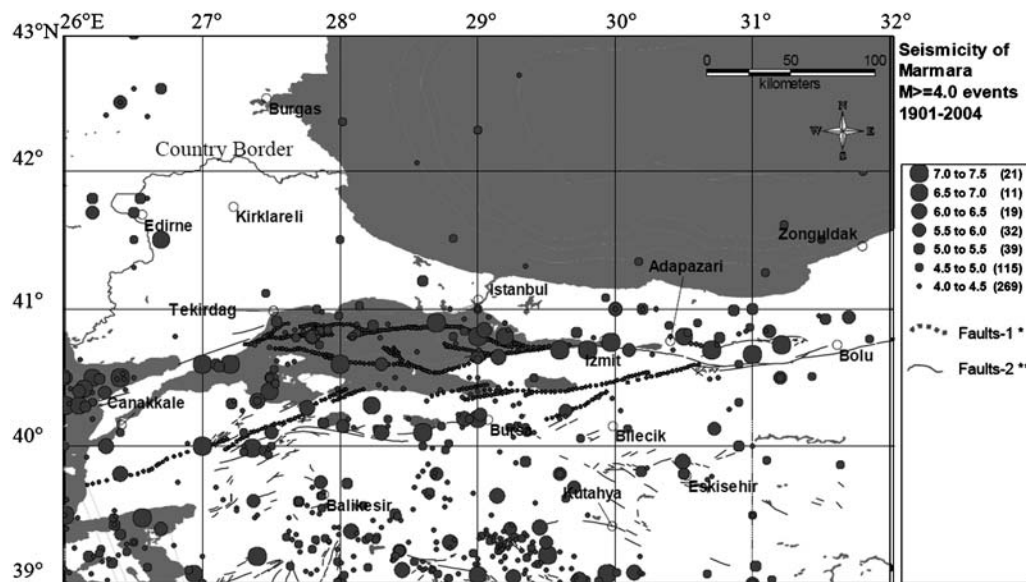


**Figure 3.** Seismicity of the Marmara region during the 103 years between 1901 and 2004. The numbers of earthquakes are given in parentheses.

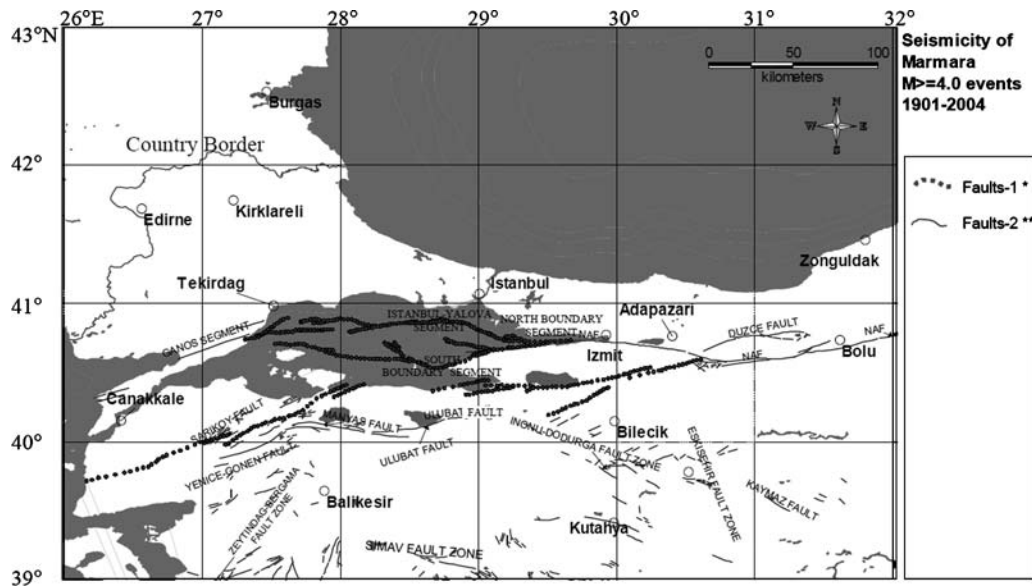


**Figure 4.** Active faults in the Marmara region (NAF).

(McClusky *et al.*, 2000). This dynamic structure pushes the Marmara region in a northerly path. The NAF system within the Marmara region can account for  $22 \pm 3$  mm/yr right-lateral slip (Straub *et al.*, 1997; McClusky *et al.*, 2000). On the basis of Le Pichon *et al.* (2001), we assigned 23 mm/yr slip-rate to major faults below the Marmara Sea; for the rest of the fault segments, the slip-rate distribution from Global Positioning System (GPS) measurements given in Straub *et al.* (1997) were used. The slip-rate distributions assigned to fault segments agree with tectonic (Barka and Kadinsky-Cade, 1988; McClusky *et al.*, 2000; Yaltirak, 2002; Seeber *et al.*, 2004; Aksoy *et al.*, 2006; Motagh *et al.*, 2007) and kinematic simulation-based (Pulido *et al.*, 2004) studies.

### General Methodology

Based on our current state of knowledge about the seismicity and tectonic environment of the Marmara basin, regional probabilistic seismic hazard analysis (PSHA) is performed using two different classes of earthquake source models: (1) a smoothed-gridded seismicity model and (2) a fault model. The first model is based on the earthquake catalog and characterizes the hazard from earthquakes between  $M$  4.0 and 6.5. The faults contribute to the hazard for earthquakes larger than  $M$  6.5. As a recurrence forecasting process, the Poisson equation (time independent) is used to estimate the probability of exceedance over finite time interval.

### Earthquake Catalog

The earthquake catalog includes events from historical and instrumental seismicity. The magnitude, epicenter coordinates, and depth of all events with  $M \geq 6.0$  are listed in Table 1 ( $M \geq 7.0$  events are in bold type). These events were

compiled from different sources (see Data and Resources section) that use different intensity scales: (1) Earthquake Research Department, General Directorate of Disaster Affairs of Turkey; (2) Kandilli Observatory, Boğaziçi University; (3) International Seismological Centre of UK; and (4) the U.S. Geological Survey. Magnitude scales of all events were converted to moment magnitude ( $M$ ) through a set of empirical equations derived based on Turkish earthquakes (Yenier *et al.*, 2008). These equations are listed in descending order of priority of the scales selected to convert to  $M$ .

$$M = 0.571M_s + 2.484, \quad 3.0 \leq M_s < 5.5 \quad (1a)$$

$$M = 0.817M_s + 1.176, \quad 5.5 \leq M_s \leq 7.7 \quad (1b)$$

$$M = 0.953M_L + 0.422, \quad 3.9 \leq M_L \leq 6.8 \quad (1c)$$

$$M = 0.764M_d + 1.379, \quad 3.7 \leq M_d \leq 6.0 \quad (1d)$$

$$M = 1.104m_b - 0.194, \quad 3.5 \leq m_b \leq 6.3 \quad (1e)$$

In compiling the catalog of events, fore- and aftershocks were removed using the declustering methodology (Gardner and Knopoff, 1974); this simple algorithm requires no tuning parameters, thus the results are easily reproducible. In addition, events before 1901 were excluded due to catalog incompleteness. For the 103 yr time period between 1901 and

Table 1  
Marmara Region Earthquakes with  $M \geq 6.0$  (A.D. 1509–1999)

Number	Year	Month	Day	Latitude	Longitude	Depth (km)	$M^*$	Approximate Rupture Length (km) <sup>†</sup>	Source <sup>‡</sup>
1	1509	9	10	40.90	28.70	-	6.7	24	1
2	1556	5	10	40.60	28.00	-	6.7	24	1
3	1625	5	18	40.30	26.00	-	6.6	21	1
4	1659	2	17	40.50	26.40	-	6.7	24	1
5	1672	2	14	39.50	26.00	-	6.6	19	1
6	1719	5	25	40.70	29.80	-	6.8	29	1
7	1737	3	6	40.00	27.00	-	6.6	19	1
8	1766	5	22	40.80	29.00	-	6.6	21	1
9	1766	8	5	40.60	27.00	-	6.8	29	1
10	1855	2	28	40.10	28.60	-	6.6	21	1
11	1894	7	10	40.70	29.60	-	6.8	26	1
12	1905	4	15	40.20	29.00	-	6.6	19	4
13	<b>1912</b>	8	10	40.60	27.20	16	<b>7.4</b>	100	4
14	<b>1919</b>	11	18	39.20	27.40	-	<b>7.0</b>	44	2
15	1928	5	3	39.64	29.14	10	6.1	7	4
16	1935	1	4	40.40	27.49	30	6.7	24	4
17	<b>1939</b>	9	22	39.07	29.94	10	<b>7.1</b>	54	4
18	1939	10	19	39.07	26.94	10	6.6	19	4
19	1942	6	16	40.80	27.8	20	6	6	4
20	1943	6	20	40.85	30.51	10	6.6	19	4
21	1944	6	25	39.05	29.26	-	6.1	7	2
22	<b>1944</b>	10	6	39.48	26.56	40	<b>7.0</b>	44	4
23	1953	3	18	39.99	27.36	10	6.6	19	1
24	1956	2	20	39.89	30.49	40	6.4	13	4
25	1957	5	26	40.67	31.00	10	6.7	24	1
26	1961	11	28	40.00	26.30	-	6.0	6	4
27	1964	10	6	40.30	28.23	34	6.9	36	2
28	1966	8	21	40.33	27.40	12	6.0	6	4
29	1967	7	22	40.70	30.70	-	6.7	24	1
30	<b>1970</b>	3	28	39.21	29.51	18	<b>7.1</b>	54	2
31	1971	5	25	39.03	29.74	24	6.1	7	3
32	1975	3	27	40.42	26.14	5	6.7	24	3
33	1976	8	25	39.30	28.80	33	6.0	6	4
34	1976	9	6	39.06	29.00	11	6.6	19	4
35	<b>1999</b>	8	17	40.76	29.97	18	<b>7.4</b>	100	5
36	<b>1999</b>	11	12	40.74	31.21	25	<b>7.2</b>	66	5

\*Moment magnitude values are converted from  $M_S$  (as given by Aki, 1983) using equation (1c).  $M \geq 7.0$  events are in bold type.

†Based on Wells and Coppersmith (1994) empirical formulations.

‡(1) Ambraseys (2006), (2) Papazachos and Papazachou (1997), (3) U.S. Council of National Seismic System (CNSS) Catalog, (4) Kandilli Observatory and Earthquake Research Institute, and (5) Gulkan and Kalkan (2002).

2004, the catalog completeness was tested by plotting the cumulative number of events against time (Al-Tarazi and Sandvol, 2007); Figure 5 depicts the distribution of all distinct events between  $M$  4.0–5.0 and  $M$  5.0–6.0. When events with magnitudes 5.0 and 6.0 are considered, these plots are approximately linear for the 103 yr period. Similar analyses were made for the magnitude intervals 4–5, 5–6, and 6+. We computed completeness levels of  $M$  4.0 or greater since 1964 and  $M$  5.0 or greater since 1901.

### Earthquake Recurrence

For the computation of smoothed-gridded seismicity, a catalog having discrete independent earthquakes was associated with the Gutenberg–Richter (GR) earthquake recur-

rence relation:

$$\log(N) = a - bM, \tag{2}$$

where  $N$  is the annual number of earthquakes of magnitude equal to or greater than  $M$ ,  $10^a$  is the mean yearly number of earthquakes of magnitude greater than or equal to zero, and  $b$  describes the relative likelihood of large and small earthquakes. As the number of larger magnitude earthquakes decreases compared to those of smaller magnitudes, the  $b$ -value increases.

For the Marmara region, the 100 yr long data set is more complete for small events than is the 2000 yr long data set and yields  $b = 0.60$ ; whereas the 2000 yr long data set results in a lower  $b$ -value and consequently assigns higher

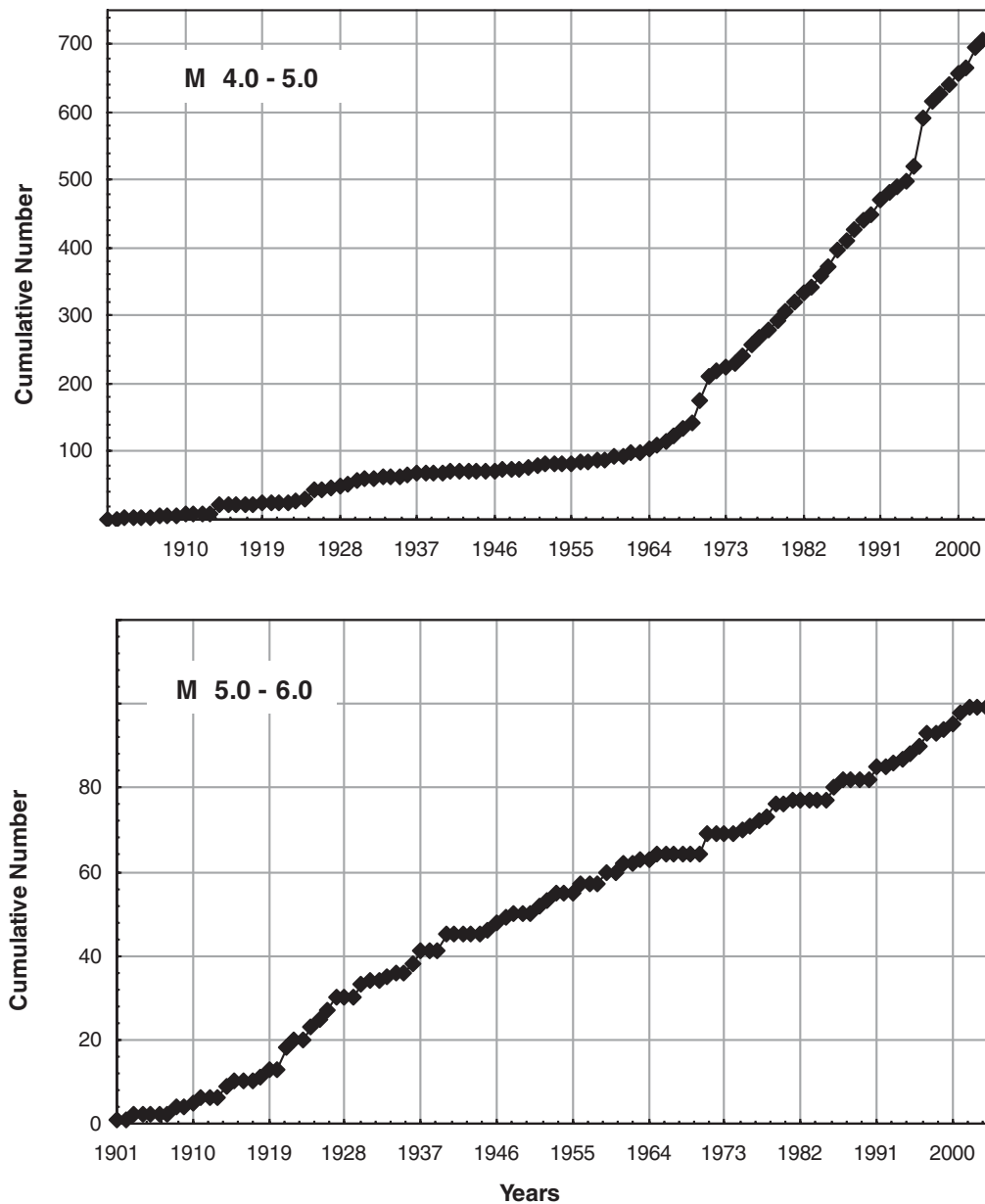


**Figure 5.** Incompleteness test for earthquakes that occurred in the Marmara region for  $M$  4–5 (upper) and  $M$  5–6 (lower) considering a 103 yr time interval (between 1901 and 2004).

mean rate of transcendence for larger events (Ambraseys, 2002). A  $b = 0.69$  for the same region considering the 100 yr long earthquake catalog with  $M \geq 5.5$  events is reported by Crowley and Bommer (2006). For the entire Marmara region, the  $b$ -value was estimated as 0.72 using maximum likelihood method (Weichert, 1980) based on the 103 yr catalog; this method accounts for variable completeness. No uncertainty associated with the  $b$ -value was considered since the single  $b$ -value calculated herein is in good agreement with the values reported in previous studies. Thereafter,  $a$  values were computed for each cell and spatially smoothed over a grid of  $0.05^\circ \times 0.05^\circ$  in latitude and longitude using two-dimensional Gaussian filters

with a decay of 50 km. Such a fine grid resulted in hazard computations at about 9600 grid sites.

#### Source Models

*Smoothed-Gridded Seismicity Model.* The contribution of background events to hazard is calculated using the smoothed-gridded seismicity model (Frankel, 1995; Kafka, 2002). This model addresses the aleatoric uncertainty in the location of future earthquakes, thus allowing spatially stationary seismicity while eliminating the subjectivity in delineation of areal sources. This seismicity model requires a declustered earthquake catalog for computation of Poissonian earthquake recurrence rates. In this model, events that

are not assigned to specific faults are assumed to be potential seismogenic sources and are spatially gridded to cells. First, we count the number of earthquakes  $n_i$  with magnitude greater than  $M_{\text{ref}}$  in each cell  $i$  of a grid with spacing of  $0.05^\circ$  in latitude and  $0.05^\circ$  in longitude. This count represents the maximum likelihood estimate of  $10^a$  for that cell (Weichert, 1980; Bender, 1983) for earthquakes above  $M_{\text{ref}}$ . The values of  $n_i$  are converted from cumulative values (number of events above  $M_{\text{ref}}$ ) to incremental values (number of events from  $M_{\text{ref}}$  to  $M_{\text{ref}} + \Delta M$ ) using the Herrmann formula (Herrmann, 1977). The grid of  $n_i$  values is then smoothed spatially by multiplying by a Gaussian function with correlation distance  $c$ . For each cell  $i$ , the smoothed value  $\tilde{n}_i$  is obtained from (Frankel, 1995)

$$\tilde{n}_i = \frac{\sum_j n_j e^{-\Delta_{ij}^2/c^2}}{\sum_j e^{-\Delta_{ij}^2/c^2}}. \quad (3)$$

In this equation,  $\tilde{n}_i$  is normalized to preserve the total number of events, and  $\Delta_{ij}$  is the distance between the  $i$ th and  $j$ th cells. The sum is taken over cells  $j$  within a distance of  $3c$  of cell  $i$ . The annual probability of exceeding specified ground motions is calculated for a grid of sites using  $\tilde{n}_i$  from equation (3). For each site, the values of  $\tilde{n}_i$  are binned by their distance from that site, so that  $N_k$  denotes the total of  $\tilde{n}_i$  values for cells within a certain distance increment of the site. Now the annual rate  $\lambda(u > u_0)$  of exceeding ground motion  $u_0$  at a specific site is determined from a sum over distance and magnitude (Frankel, 1995)

$$\lambda(u > u_0) = \sum_k \sum_l 10^{\log(N_k/T) - b(M_l - M_{\text{ref}})} \times P(u > u_0 | D_k, M_l), \quad (4)$$

where  $k$  is the index for the distance bin, and  $l$  is the index for

the magnitude bin;  $T$  is the time in years of the earthquake catalog used to determine  $N_k$ . The first factor in the summation is the annual rate of earthquakes in the distance bin  $k$  and magnitude bin  $l$ .  $P(u > u_0 | D_k, M_l)$  is the probability that  $u$  at the site will exceed  $u_0$ , for an earthquake at distance  $D_k$  with magnitude  $M_l$  ( $D_k$  is fixed for each bin). This probability is dependent on the attenuation relation and the standard deviation (variability) of the ground motion for any specific distance and magnitude. For this model, values are computed from the magnitude 4.0 and larger earthquakes since 1901.

**Segmented Fault Source Model.** This model is based on the assumption that large earthquakes occurring in small areas are likely to belong to the same seismogenic fault or a homogenous system of faults. This implies that the seismicity is concentrated on fault planes. In order to utilize the contribution of the fault sources to regional seismic hazard, four aspects of each source are examined. These are: (a) style-of-faulting, (b) location and orientation, (c) slip rate, and (d) maximum magnitude earthquake expected (Petersen *et al.*, 2000). All faults that were included in the evaluation are judged with confidence as active faults with reported slip rates greater than or equal to 10 mm/yr; other active faults having slip rates less than 10 mm/yr were not included. For the faults below the Marmara Sea, we used fault segmentation data from Le Pichon *et al.* (2003) and Armijo *et al.* (2005). The remainder of the faults was taken from the active fault map of Turkey (Saroglu *et al.* 1992) with the caveat that this map is in the process of being updated. As shown in Figure 6, the region's complex fault system is modeled with 48 fault segments and each is assumed to rupture independently. The properties of each fault segment are tabulated in Table 2.

For nonvertical faults, dip angle is an important parameter to determine the average fault depth and the projected

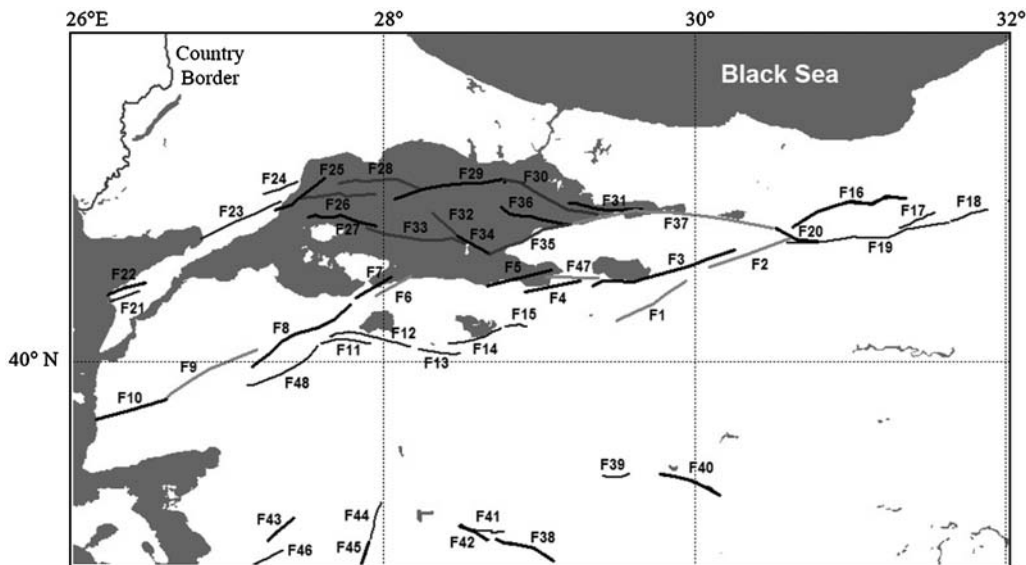


**Figure 6.** Fault segmentation model for the Marmara region (see Table 2 for fault names and their activity rates).

Table 2  
Characteristic Attributes of Fault Segmentation Model

Fault Segment	Length (km)	Characteristic Event ( $M$ )	Slip-Rate (mm/yr)	Activity Rate (Earthquake/yr)	Fault Segment	Length (km)	Characteristic Event ( $M$ )	Slip-Rate (mm/yr)	Activity Rate (Earthquake/yr)
F1	45	7.0	20	0.0073	F25	31	6.8	20	0.0095
F2	48	7.0	20	0.0070	F26	44	7.0	20	0.0074
F3	82	7.3	20	0.0049	F27	42	7.0	20	0.0077
F4	31	6.8	20	0.0094	F28	51	7.1	23	0.0077
F5	36	6.9	20	0.0085	F29	62	7.2	23	0.0068
F6	22	6.7	20	0.0119	F30	51	7.1	23	0.0077
F7	28	6.8	20	0.0101	F31	20	6.6	23	0.0148
F8	63	7.2	20	0.0058	F32	16	6.5	20	0.0150
F9	58	7.1	20	0.0062	F33	57	7.1	20	0.0062
F10	40	7.0	20	0.0079	F34	20	6.6	20	0.0128
F11	28	6.8	20	0.0101	F35	41	7.0	20	0.0077
F12	46	7.0	20	0.0072	F36	36	6.9	20	0.0085
F13	21	6.6	20	0.0121	F37	112	7.5	23	0.0045
F14	29	6.8	20	0.0099	F38	36	6.9	18	0.0076
F15	21	6.7	20	0.0121	F39	15	6.5	18	0.0140
F16	66	7.2	20	0.0056	F40	37	6.9	18	0.0075
F17	21	6.6	20	0.0122	F41	30	6.8	18	0.0088
F18	21	6.6	20	0.0124	F42	10	6.3	18	0.0185
F19	90	7.3	20	0.0046	F43	20	6.6	15	0.0096
F20	26	6.7	20	0.0107	F44	22	6.7	15	0.0089
F21	19	6.6	20	0.0133	F45	15	6.5	15	0.0116
F22	23	6.7	20	0.0114	F46	20	6.6	15	0.0096
F23	49	7.1	10	0.0034	F47	30	6.8	20	0.0097
F24	33	6.9	10	0.0045	F48	46	7.0	20	0.0072

distance on the grid to be used in the GMPEs. Because down-dip width and depth data for each fault are not available to accurately determine the actual subsurface source geometry, some of the planar sources were approximated as linear sources (i.e.,  $90^\circ$  dip is assumed for strike-slip faults). Also, 10 km depth is assigned to those faults where reliable depth information is not available. Also listed in Table 2 are the approximate slip-rates broadly described from GPS measurements because only three fault segments: Izmit, Düzce and Ganos, were studied in detail by paleoseismological methods to be able to assess the long-term slip-rates. Most of the faults that are labeled active are mainly mapped on the basis of the morphological studies and with simple spatial correlations with recent known earthquakes. These issues will remain as constraints on the results presented until more reliable data on the subsurface geometry and slip rates for faults become available.

In interpreting our fault segmentation model in Figure 6, which primarily relies on seismotectonic studies along with recurrence and locations of historical events, it should be emphasized that geometry and recurrence are not totally independent of each other. If a fault is modeled with several small segments instead of fewer large segments, the maximum magnitude will be lower, and a given slip-rate will require many more small earthquakes to accommodate a cumulative seismic moment.

For the segmented fault source model, available historical and instrumented data are not sufficient to determine whether the GR model or characteristic earthquake (CE) model or hybrid model (Youngs and Coppersmith, 1985) is more appro-

priate. Therefore, two different models (GR and CE) were placed within the logic tree with equal weights. In the CE model, each of the fault segments considered is assumed to be capable of rupturing independently and producing the maximum magnitude earthquake ( $M_{\max}$ ) based on fault length and potential rupture depth (Aki, 1983; Schwartz and Coppersmith, 1984). It should be noted that  $M_{\max}$  denotes the maximum characteristic magnitude.  $M_{\max}$  for each fault segment is computed through empirical relations (Wells and Coppersmith, 1994) and cross-checked with the neighborhood historical events. To account for the uncertainties in  $M_{\max}$  values,  $M_{\max}$  is allowed to float along each fault segment in three limits as  $M_{\max} - \sigma$ ,  $M_{\max}$ ,  $M_{\max} + \sigma$ , and  $\sigma$  is the dispersion in statistical modeling of  $M_{\max}$  and taken as 0.3 on the basis of Wells and Coppersmith (1994).

For the faults, we used the following seismic moment formula to find the activity rate of the characteristic event, i.e., number of earthquake per year or reciprocal of its recurrence interval from

$$M_0 = \mu AD, \quad (5)$$

where  $M_0$  is the seismic moment of the characteristic earthquake. The rigidity or shear modulus of the crust is represented by  $\mu$  and is taken as  $3.0 \times 10^{11}$  dyne/cm<sup>2</sup>.  $A$  is the area of the rupture plane (in cm<sup>2</sup>), and  $D$  is the slip on the plane (in cm). Time derivative of equation (5) results in a moment rate as a function of slip-rate

$$M'_0 = \mu AS, \quad (6)$$

where  $M'_0$  is the moment rate, and  $S$  is the slip rate. The seismic moment can be obtained through moment magnitude,  $M$ , from the relation given by Hanks and Kanamori (1979)

$$M = 2/3 \log M_0 - 10.7 \quad (7)$$

By rewriting equation (7), we obtain seismic moment as

$$\log_{10}(M_0) = 1.5M + 16.05 \quad (8)$$

and the activity rate of earthquakes above a minimum magnitude,  $M_{\min}$ , from

$$N(M_{\min}) = \frac{\mu AS}{\text{mean}(M_0/\text{earthquake})} \quad (9)$$

On the basis of these formulas, the activity rate for each fault segment was computed and is listed in Table 2.

The GR model requires computation of  $a$  value for each fault segment, therefore, buffer zones with radius of 10–15 km were introduced around each fault segment, and events within each zone were counted. If one event was counted for one buffer zone, it was not included in any other zones although it might fall within their radius.

#### Ground-Motion-Prediction Equations

In the post-1999 period, many ground motion records were recorded in Turkey. These new data were combined with the existing national ground motion library to develop a GMPE to be used for regional hazard assessments (Gülkan and Kalkan, 2002). The GMPE of Gülkan and Kalkan has the same functional form as the GMPE of Boore *et al.* (1997) but with different coefficients; this model was updated later by

considering a larger data set (Kalkan and Gülkan, 2004). In the study presented herein, three NGA relations (Boore and Atkinson, 2008; Campbell and Bozorgnia, 2008; Chiou and Youngs, 2008) are used in addition to the GMPE of Kalkan and Gülkan (2004) to compute the ground motions at distances less than 200 km. The NGA equations have been derived for shallow crustal earthquakes from a data set that includes some Turkish strong-motion records. These equations are found to be applicable for Europe and the Middle East (Stafford *et al.*, 2008). Figure 7 compares the attenuation curves based on four different GMPEs computed for PGA, spectral acceleration (SA) at 0.2 sec, and SA at 1.0 sec. These curves correspond to an  $M$  7.0 event on a strike-slip fault, and site condition is firm-rock ( $V_{S30} = 760$  m/sec). Note that in Kalkan and Gülkan's GMPE the larger of the two horizontal components for each record was processed in the regression, whereas all the NGA equations use the geometric mean of the two horizontal components, which is consistently smaller. For consistency, PGA, SA at 0.2 sec, and 1.0 sec predictions from KG04 were first adjusted by 0.9, 0.9, and 0.85, respectively, and then plotted in Figure 7. These factors, relating maximum horizontal component to the geometric mean of the two horizontal components, were taken from Campbell and Bozorgnia (2008). As shown, the three NGA relations produce similar results. For PGA and SA at 0.2 sec, Kalkan and Gülkan's GMPE yields slightly lower acceleration values within 5 km of fault rupture, whereas its predictions are comparable in the intermediate distances (between 5 to 25 km). For SA at 1.0 sec, Kalkan and Gülkan's GMPE estimates larger acceleration values at distances larger than 5 km as compared to the predictions of the NGA relations.

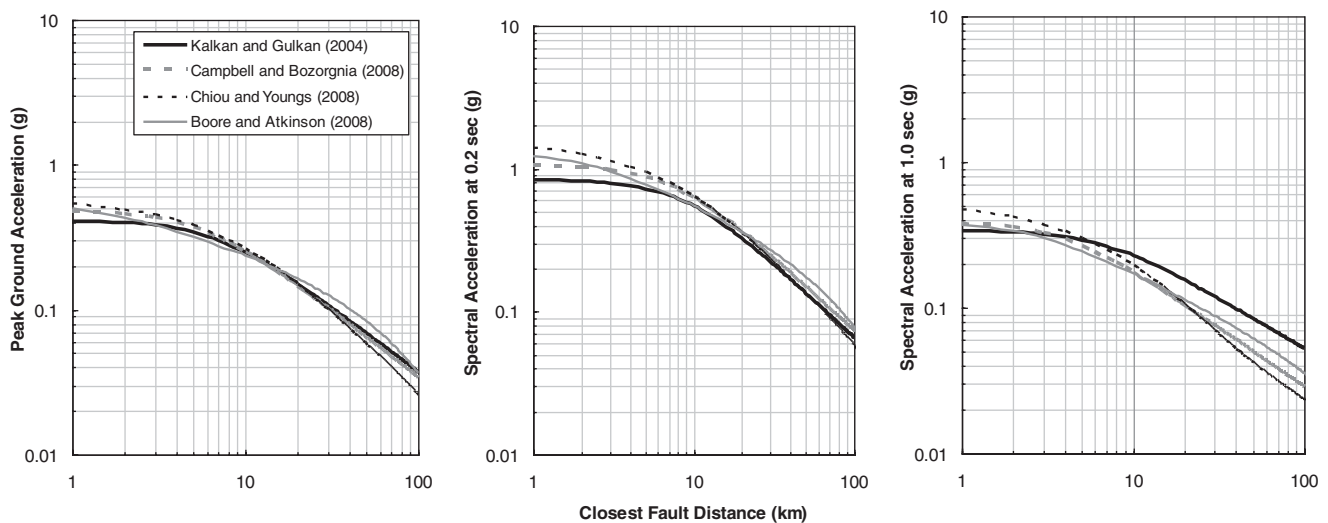


**Figure 7.** Comparison of ground motion predictions from Kalkan and Gülkan (2004) GMPE to three NGA relations (Boore and Atkinson, 2008; Campbell and Bozorgnia, 2008; Chiou and Youngs, 2008). Plots are for PGA (left panel), SA at 0.2 sec (middle panel), and SA at 1.0 sec (right panel). Ground-motion prediction is based on an  $M$  7.0 scenario event on a strike-slip fault (with depth of 2.0 km) and at a uniform firm-rock site ( $V_{S30} = 760$  m/sec).

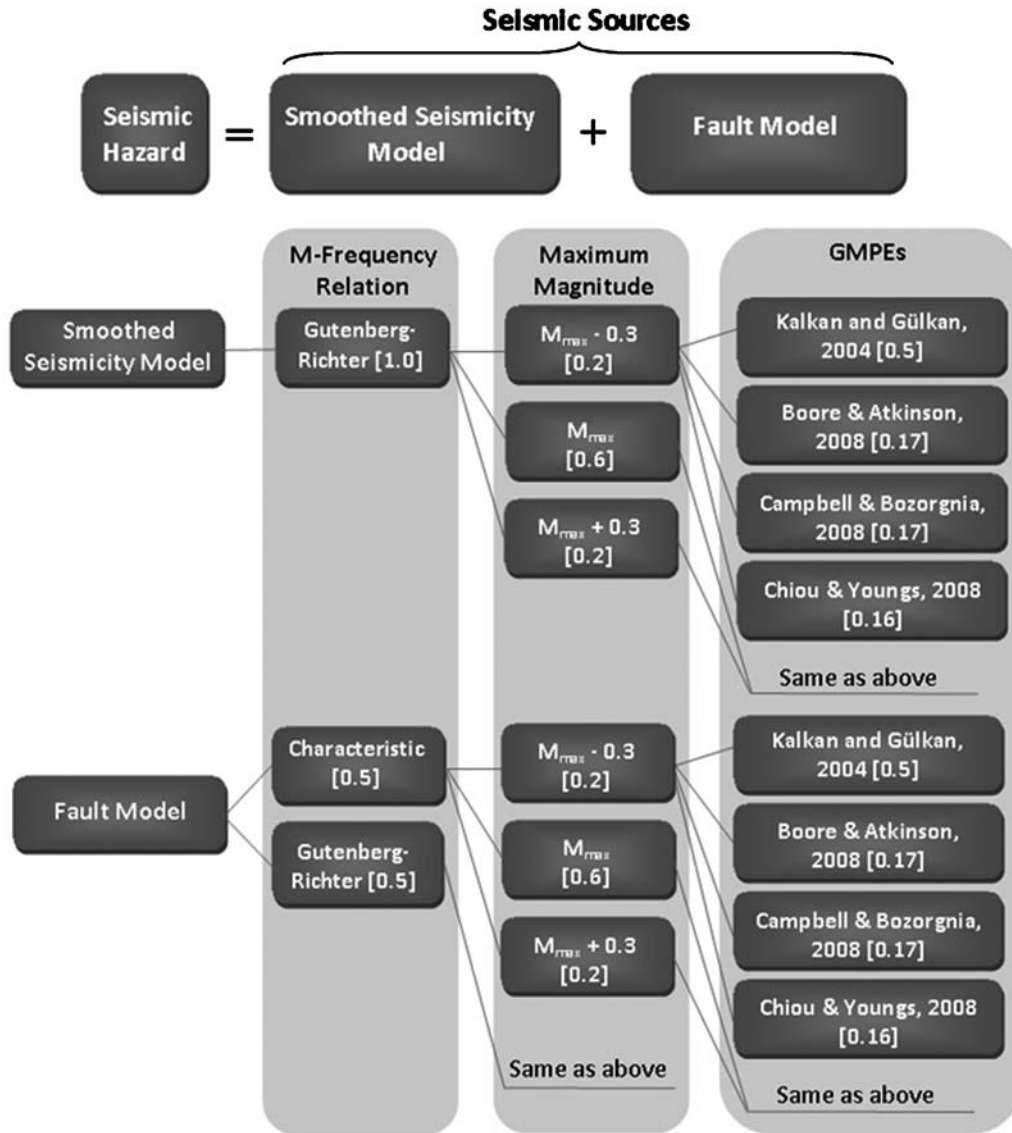


**Figure 8.** Logic tree established for seismic hazard analysis; values in brackets indicate the assigned weight to each cell;  $M_{max}$  stands for maximum magnitude.

Logic Tree

The logic tree constructed for hazard computations is shown in Figure 8. For smoothed seismicity model, the tree has 12 branches. For the fault source model, the tree has 24 branches. The weight assigned to the local GMPE is set equal to total weight of the three NGA relations. All relative weights are subjective and based on what we consider to be defensible judgment.

Seismic Hazard Results

The seismic hazard is computed for PGA and SA ordinates at 0.2 sec and 1.0 sec for the uniform firm-rock site condition ( $V_{S30} = 760$  m/sec). The 0.2 and 1.0 sec spectral periods are selected because they are frequently used to construct a smooth design spectrum; an appropriate procedure to obtain

a smooth design spectrum from a uniform hazard spectrum is given in the Federal Emergency Management Association (FEMA) 356 guidelines (ASCE, 2000). Seismic hazard for the Marmara region was computed for two ground motion levels having 2% and 10% probabilities of exceedance in 50 yr and corresponding to return periods of about 2475 (annual probability of exceedance = 0.000404) and 475 yr (annual probability of exceedance = 0.0021), respectively. Figures 9–11 render the mean seismic hazard computed for PGA, SA at 0.2 sec, and SA at 1.0 sec for 2% and 10% probability levels. The distribution of PGA and SA ordinates, shown by the color gradient, indicates a broader scattering of higher acceleration values toward the south and east of the Marmara region. For the 2475 yr return period, the maximum PGA (Fig. 9) at a uniform firm-rock site is computed as 1.5 g; PGA diminishes to 0.8 g when the return period is set to 475 yr.

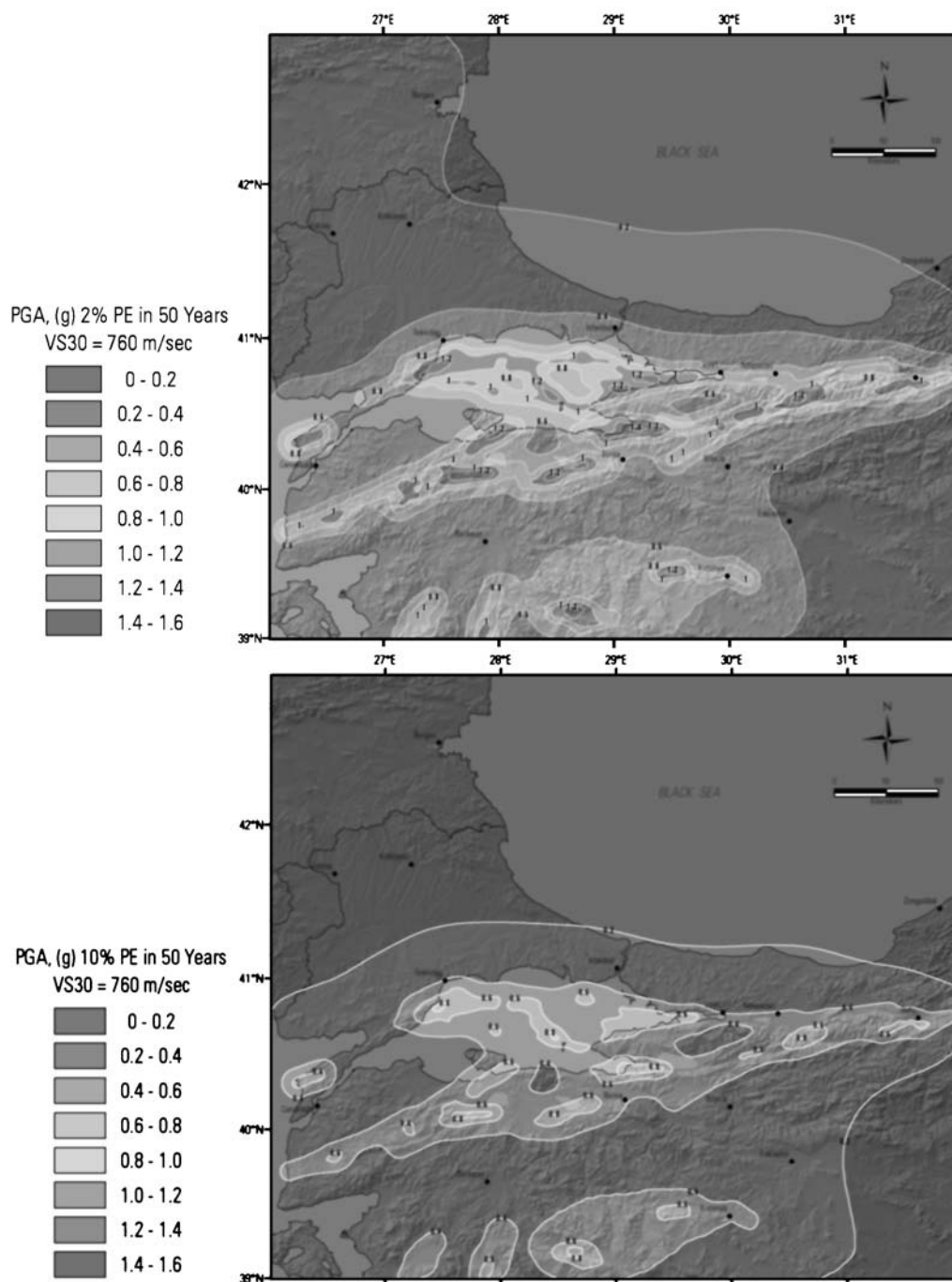


**Figure 9.** Seismic hazard map of the Marmara region for PGA for uniform firm-rock site condition considering 2% (top panel) and 10% (bottom panel) probability of exceedance in 50 yr.

Such high values of PGA are observed in the vicinity of fault segments along the branch of the NAF zone extending into the Marmara Sea. This zone of large ground motions also corresponds to areas where large numbers of 4+ events have occurred since 1901. At the same locations, the maximum SA at 0.2 sec (Fig. 10) is computed as 2.8 g and 1.8 g at the return period of 2475 and 475 yr, respectively. The maximum SA at 1.0 sec (Fig. 11) is computed as 1.5 g for a 2475 yr return period and 0.8 g for a 475 yr return period.

The hazard maps presented in Figures 9–11 are for a uniform firm-rock site condition ( $V_{S30} = 760$  m/sec). To obtain motions for average stiff-soil site ( $V_{S30} = 360$  m/sec) and soft-soil site ( $V_{S30} = 180$  m/sec), the mapped values should be modified. It is not possible to provide a constant modification factor to transfer the hazard values computed for  $V_{S30} = 760$  m/sec to those at  $V_{S30} = 360$  m/sec or 180 m/sec because the three NGA relations utilized have nonlinear site correction term; that is, site amplification decreases with

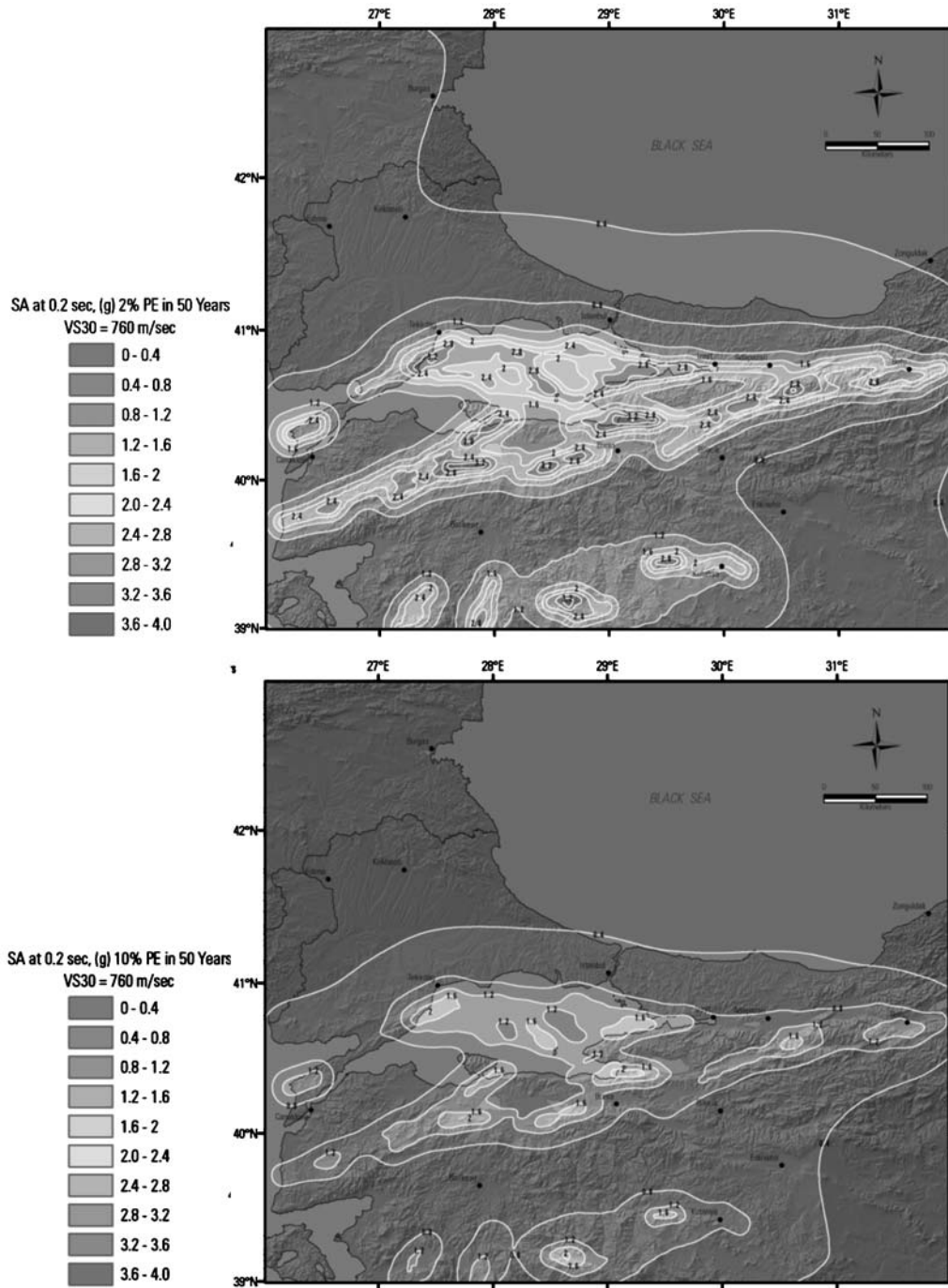


**Figure 10.** Seismic hazard map of the Marmara region for spectral acceleration at 0.2 sec for uniform firm-rock site condition considering 2% (top panel) and 10% (bottom panel) probability of exceedance in 50 yr.

increasing ground motion intensity as surface materials reach their limit strength and start behaving nonlinearly. The difference between a linear and nonlinear site correction term affects the stronger ground motions. In order to predict the ground motion at soil and soft-soil sites, we computed the amplification factors (by taking the ratio of hazard results for a particular  $V_{S30}$  to those for  $V_{S30} = 760$  m/sec) at every grid point and projected them on a series of site amplification maps in Figures 12 and 13. These maps are generated for PGA and

SA at 0.2 sec, and SA at 1.0 sec considering ground-motion level at 2% and 10% probability of exceedance in 50 yr. For both ground motion levels, site amplification factors for  $V_{S30} = 180$  m/sec are almost unity at the locations where the high PGA values are computed. For  $V_{S30} = 180$  m/sec, Kalkan and Gülkan’s GMPE yields a constant amplification factor of 1.3 independent of the PGA level. At the PGA level of 0.3 g and higher, NGA relations yield site amplification factors less than unity; therefore, combination of four GMPE

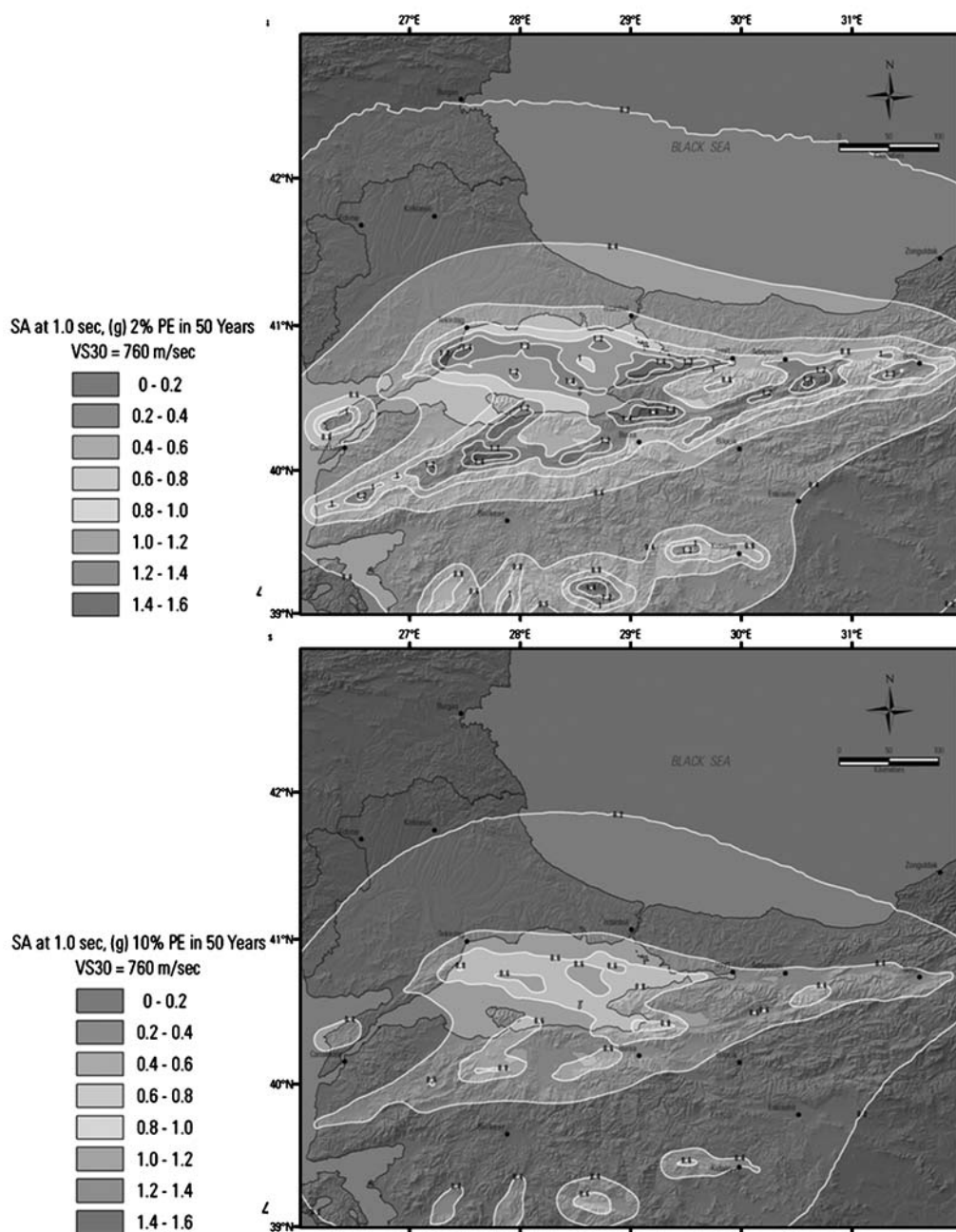


**Figure 11.** Seismic hazard map of the Marmara region for spectral acceleration at 1.0 sec for uniform firm-rock site condition considering 2% (top panel) and 10% (bottom panel) probability of exceedance in 50 yr.

within the logic tree results in no site amplification around the major fault lines. The same applies for SA at 0.2 sec. However, for SA at 1.0 sec, NGA relations yield amplification factors greater than unity, thus, soft-soil sites around the major fault lines are expected to experience a minimum 1.6 times higher ground motion as compared to the uniform firm-rock sites considering 2% probability of exceedance in 50 yr. In general, nonlinearity phenomena result in a shift of the energy to longer response periods. Comparisons between Figures 12 and 13 show that site amplification factors computed for 10% probability of exceedance level are higher than those for 2%

probability of exceedance level because nonlinearity is more pronounced for higher PGA and spectral acceleration values at 2% probability of exceedance level. Note that about 20% deamplification is predicted by NGA formulas at higher frequencies such as 0.2 sec for soft-soil compared to rock when ground motions are high.

#### Seismic Hazard of the Istanbul Metropolitan Area

The northern segments of the Marmara Sea faults are about 10–15 km from the southern coastline of Istanbul

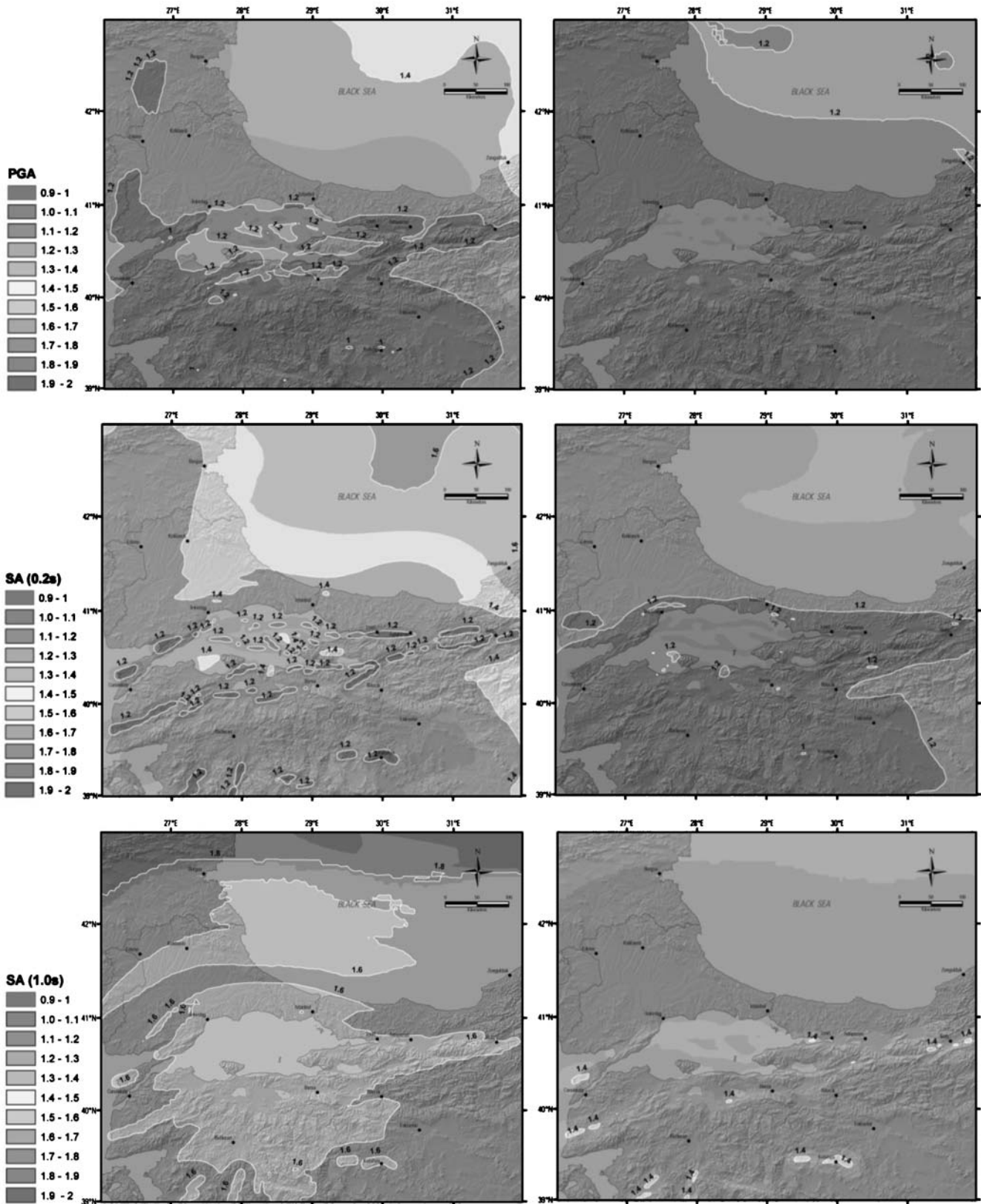


**Figure 12.** Site amplification map of the Marmara region for PGA, SA (0.2 sec), and SA (1.0 sec) considering 2% probability of exceedance. Ratio of ground-motion estimate between  $V_{S30} = 180$  m/sec and  $V_{S30} = 760$  m/sec (left panels). Ratio of ground-motion estimate between  $V_{S30} = 360$  m/sec and  $V_{S30} = 760$  m/sec (right panels).

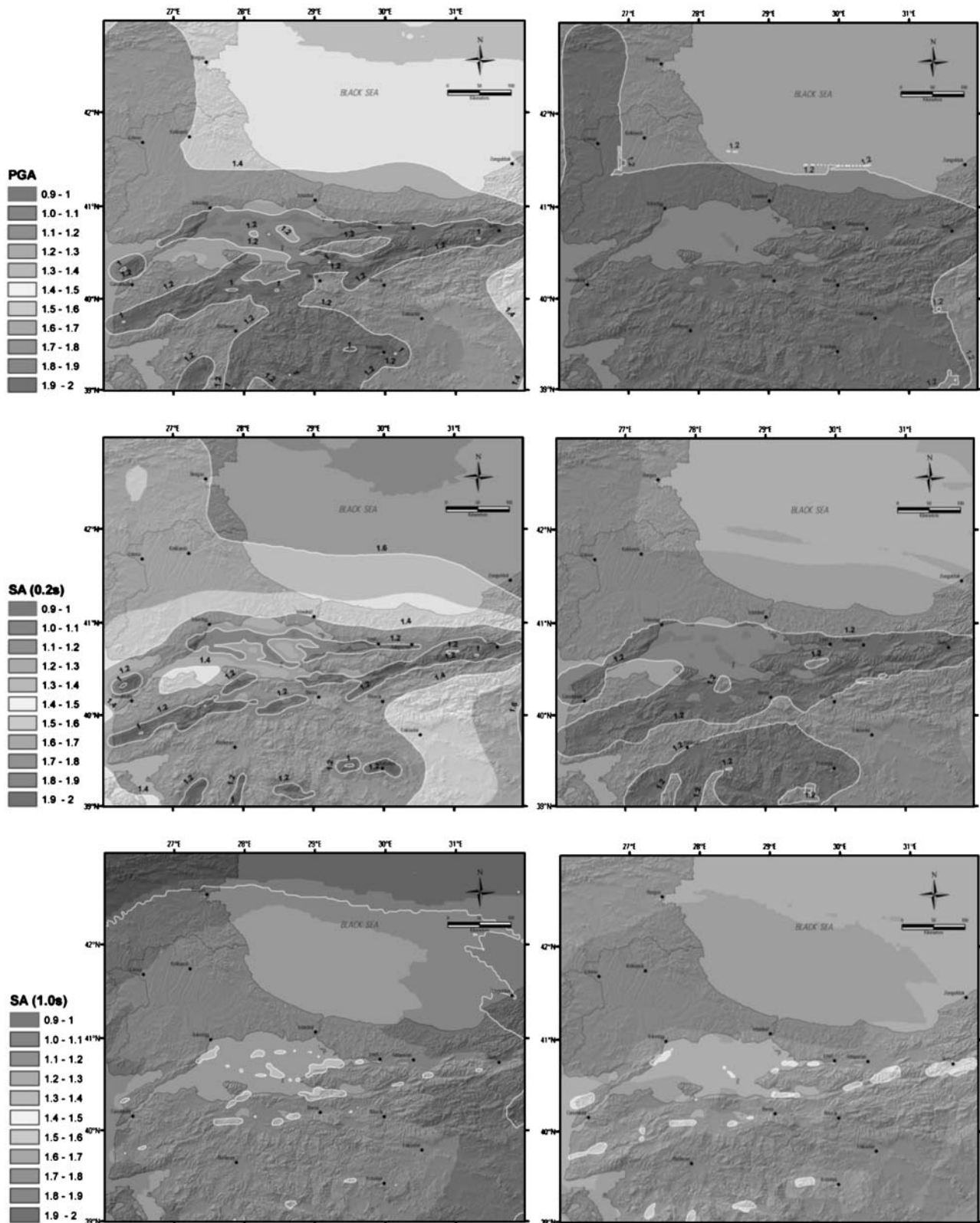


**Figure 13.** Site amplification map of the Marmara region for PGA, SA (0.2 sec), and SA (1.0 sec) considering 10% probability of exceedance. Ratio of ground motion estimate between  $V_{S30} = 180$  m/sec and  $V_{S30} = 760$  m/sec (left panels). Ratio of ground motion estimate between  $V_{S30} = 360$  m/sec and  $V_{S30} = 760$  m/sec (right panels).

proper (Fig. 4), while two-thirds of the city remains within 20–30 km radius of fault segments F29 and F30 (Fig. 6). These fault segments when ruptured independently have the potential to generate an event with magnitude greater than 7 (see Table 2 for their characteristic magnitudes). Intense PGA level is expected particularly in southern parts of Istanbul where the Istanbul Strait opens to the Marmara Sea. The level of shaking gradually diminishes toward the north. The predicted PGA ranges between 0.3 and 0.4  $g$  for 475 yr return period in southern parts of Istanbul; estimated PGA increases to as much as 0.45  $g$  on the shoreline west of Istanbul. The 2475 yr return period pushes this envelope from 0.5 to 0.7  $g$  level. The results of the previous study by Gülkan *et al.* (1993), constituting the fundament of the regulatory seismic zoning map of Turkey, reveal PGA distribution about 0.4  $g$  around Istanbul metropolitan area for 475 yr return period, in good agreement with our predictions. For the Istanbul metropolitan area seismic hazard curves are plotted in Figure 14 for PGA, SA at 0.2 sec, and SA at 1.0 sec by considering a uniform firm-rock, soil, and soft-soil sites. The two horizontal reference lines drawn indicate 2% and 10% probability levels.

For the Istanbul  $c$  area, site-dependent design spectra are computed next by using the PSHA-based uniform hazard spectra following the FEMA-356 procedure. The smooth design spectrum for each of three site categories are produced for 10% probability of exceedance in 50 yr; the resultant smooth spectra are shown in Figure 15. The design spectra based on the regulatory Turkish Seismic Code (TSC; Ministry of Public Works and Settlement, 2007) are also plotted on the same figure for comparison. In this figure, Z4, Z3, and Z2 denote the TSC-2007 site classifications; they roughly correspond to  $V_{S30} = 180, 360,$  and  $760$  m/sec, respectively.

TSC-2007 design spectra well envelope the smooth design spectra and remain on the conservative side. It should be noted that TSC-2007 does not consider distance to fault as a parameter in constructing the design spectrum and assumes that the design spectrum based on a specific site category is invariant within a seismic zone; Turkey is divided into five seismic zones, and the southern part of Istanbul is located in zone 1 designated as the most active seismic zone. The PSHA results presented here and the previous study by Kalkan and Gülkan (2004) suggest that Turkish code-based spectrum should have distance dependence similar to the International Building Code (International Conference of Building Officials [ICBO], 2006) to achieve realistic design spectral values consistent with regional hazard conditions. For distances close to faults, design spectrum may be constructed as the lower spectral values computed from a deterministic-based approach (where a characteristic event dominates the hazard) and probability-based approach; for farther distances the probabilistic-based approach may govern the design spectrum. A suite of deterministic-based design spectra have been already developed for Turkey (Kalkan and Gülkan, 2004).

## Conclusions

This paper presents a reassessment of the seismic hazard in the Marmara region on the basis of recent findings on sea bottom surveys and enhanced ground motion library from recent national events. All potential sources of seismic activity that might contribute to ground motions were identified and characterized by examining geologic, tectonic, historic, and instrumental evidence. The methodology applied here is similar to that used in the development of the most recent U.S. seismic hazard maps. Two models of seismic sources were combined and employed with different GMPEs for the

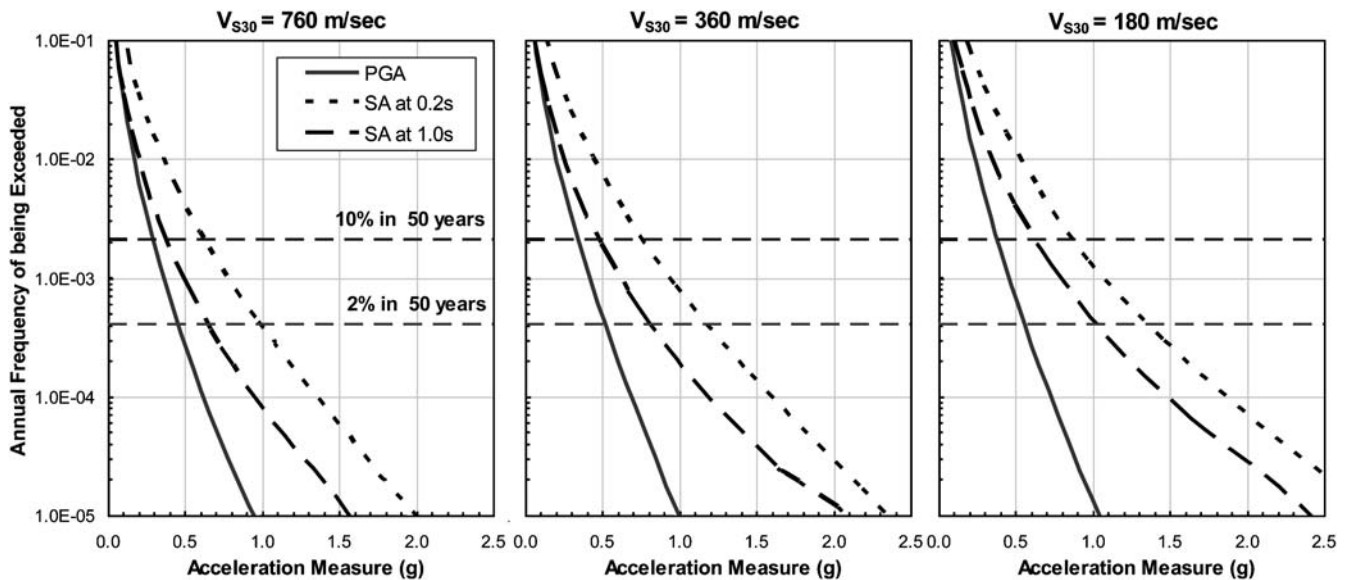


**Figure 14.** Seismic hazard curves for the Istanbul metropolitan area computed for PGA, SA at 0.2 sec, and SA at 1.0 sec for uniform firm rock ( $V_{S30} = 760$  m/sec), soil ( $V_{S30} = 360$  m/sec), and soft-soil ( $V_{S30} = 180$  m/sec) sites. Horizontal dashed lines identify 2% and 10% probability of a given acceleration level being exceeded.

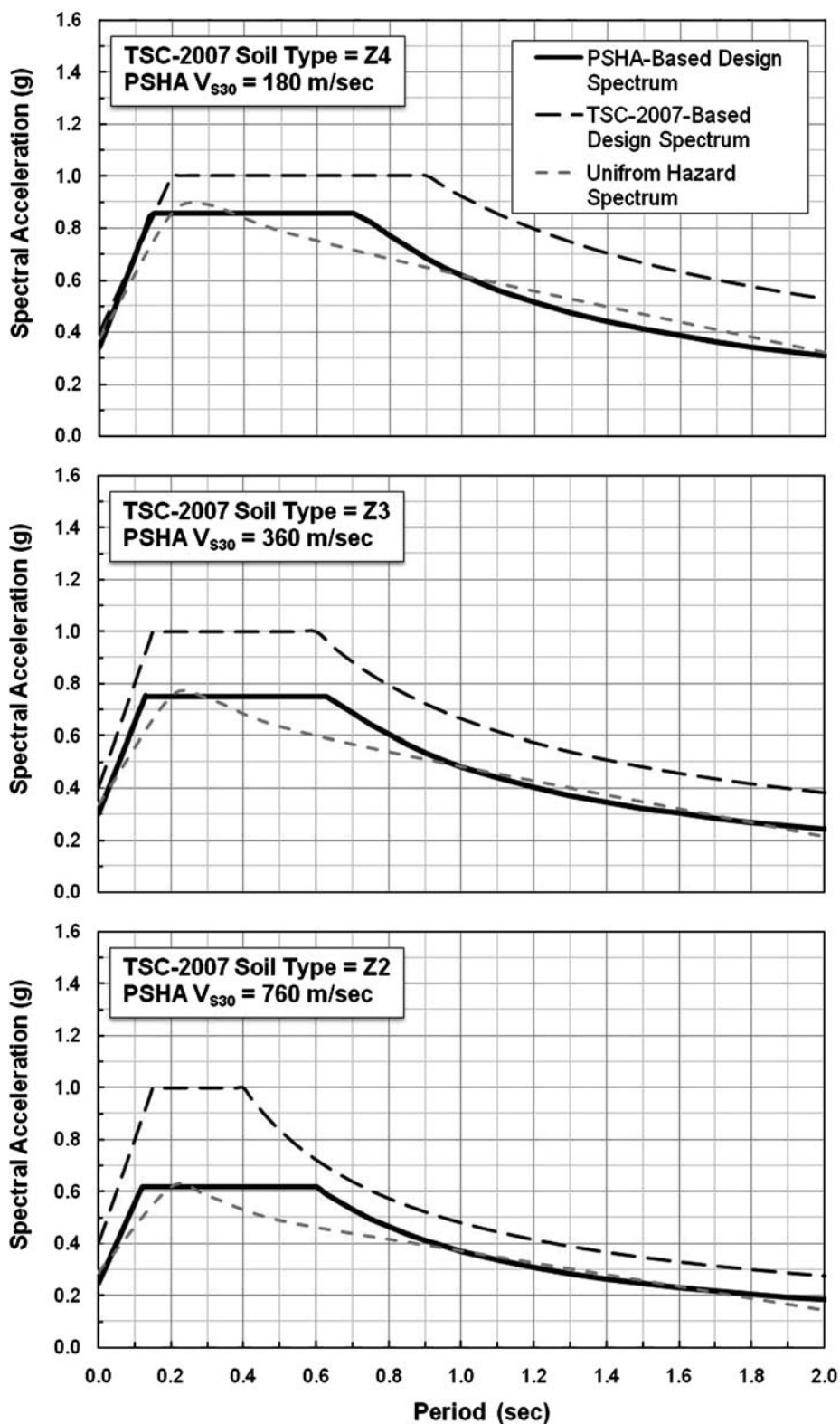


**Figure 15.** Comparison of PSHA-based smooth design spectrum (10% probability of exceedance in 50 yr) constructed on uniform hazard spectrum with Turkish Seismic Code (2007) design spectrum for rock, soil, and soft-soil site conditions (TSC site classes are Z2, Z3, Z4, respectively). Damping ratio is 5%.

assessment of hazard quantified in terms of peak ground acceleration and spectral accelerations at 0.2 and 1.0 sec with 2% and 10% probability of exceedance in 50 yr. Confidence of time-dependent models is inevitably hampered by short-term completeness of the earthquake catalog, and as a result temporal occurrence of earthquakes was assumed to be Poissonian; because of that our model represents an upper bound compared to time-dependent models. Hazard maps were computed for generic rock site conditions; for soil and soft-soil sites, a set of amplification maps is provided.

The reliability of the hazard analyses conducted here depends primarily on precision with which uncertainty in magnitude, epicenter, recurrence, fault segmentation, and their cross effects can be identified and characterized. For instance, the maximum magnitude at each fault segment was estimated from the fault length and approximate slip rates. In order to account for the associated uncertainties, maximum magnitude is allowed to float along each fault segment. This treatment results in enhanced hazard level especially for long return periods (e.g., 2475 yr), while its influence remains marginal for short return periods (e.g., 475 yr). The uncertainty in recurrence is also a factor because of the many big events in the 1999–present period. We have ignored the faults with less than 10 mm/yr average slip. In addition, we did not model faults as unsegmented as another branch in the logic tree. Considering them in PSHA may increase the hazard in the region.

Results in this study show that for the 475 yr return period, PGA may reach to as much as a 0.4 g level in the southern areas of Istanbul and the Yalova region and 0.5 g level around the shoreline to the west of the metropolitan area at a closest distance of about 10 km to the active Marmara Sea faults. PGA increases to the 0.8 g level at much closer distances near the fault segments. In the Istanbul downtown area, the average PGA is expected to measure at 0.4 g for 10% probability of exceedance in the next 50 yr. Our analyses for the Istanbul metropolitan area lack very fine grid-spacing, and the results presented herein are intended to give a general perspective on the anticipated level of shaking.

The principal differences of the study described here and the previous studies focused on the Marmara region (e.g., Atakan *et al.*, 2002; Erdik *et al.*, 2004) are that the GMPE developed from indigenous sources has been given preponderance in the weighting. The characteristics attributed to the seismogenic sources and use of NGA relations are also major improvements. The new maps (Figs. 9–11) generally show 10% to 15% increase for PGA, 0.2 sec, and 1.0 sec spectral acceleration across much of Marmara compared to previous regional hazard maps.

The seismic hazard maps provided here are intended to shed some light on future assessments of risk to structures in the defined Marmara region and, we hope, serve as a reminder to improve design and construction practices to minimize losses of life and property.

## Data and Resources

Digital data of hazard curves for the entire Marmara region including the Istanbul metropolitan area and hazard maps presented herein can be viewed in color and downloaded from [www.erolkalkan.com/Marmara\\_Research](http://www.erolkalkan.com/Marmara_Research) (last accessed June 2009). Seismic hazard maps are also integrated with the 3D-Earth model at [www.erolkalkan.com/MIM](http://www.erolkalkan.com/MIM) (last accessed June 2009) to provide an interactive interface. Events that use different intensity scales compiled from different sources are the Earthquake Research Department, General Directorate of Disaster Affairs of Turkey (<http://angora.deprem.gov.tr/ivmekataloglaren.htm>, last accessed June 2009); Kandilli Observatory, Boğaziçi University (<http://www.koeri.boun.edu.tr/sismo/Mudim/katalog.asp>, last accessed June 2009); International Seismological Centre (<http://www.isc.ac.uk/doc/products/catalogue.html>, last accessed June 2009); and the U.S. Geological Survey (<http://neic.usgs.gov/neis/epic/>, last accessed June 2009).

## Acknowledgments

We wish to thank Tom Parsons for providing us the coordinates of fault segments under the Marmara Sea and Steve Harmsen for his generous support on the latest version of the USGS seismic hazard code and also for reviewing this article. Special thanks are extended to Luke J. Blair who plotted the maps in a GIS environment, Thomas Holzer, Vladimir Graizer, and Tianqin Cao for their insightful reviews. Comments and suggestions by Julian J. Bommer, Fleur O. Strasser, and an anonymous reviewer were helpful in improving the technical quality of the paper.

## References

- Aki, K. (1983). Seismological evidence in support of the existence of characteristic earthquakes, *Earthquake Notes* **54**, 60–61.
- Aksoy, M. E., M. Meghraoui, M. Ferry, Z. Çakir, S. Akyüz, V. Karabacak, and E. Altunel (2006). Fault characteristics, segmentation and paleoseismology along the 9 August 1912 Ganos earthquake-rupture (North Anatolian Fault, Turkey), *Geophys. Res. Abstr.* **8**, 10002.
- Al-Tarazi, E., and E. Sandvol (2007). Alternative Models of Seismic Hazard Evaluation along the Jordan—Dead Sea Transform, *Earthq. Spectra* **32**, no. 1, 1–19.
- Ambraseys, N. N. (1970). Some characteristic features of the Anatolian fault zone, *Tectonophysics* **9**, 143–165.
- Ambraseys, N. N. (2002). The seismic activity of the Marmara region over the last 2000 years, *Bull. Seismol. Soc. Am.* **92**, no. 1, 1–18.
- Ambraseys, N. N. (2006). Comparison of frequency of occurrence of earthquakes with slip rates from long-term seismicity data: The cases of Gulf of Corinth, Marmara Sea and Dead Sea Fault Zone, *Geophys. J. Int.* **165**, 516–526.
- American Society of Civil Engineers (ASCE) (2000). Prestandard and Commentary for the Seismic Rehabilitation of Buildings, prepared for the SAC Joint Venture, Federal Emergency Management Agency, *FEMA-356*, Washington D.C.
- Armijo, R., B. Meyer, S. Navarro, G. King, and A. Barka (2002). Asymmetric slip partitioning in the Marmara Sea pull-apart: A clue to propagation processes of the North Anatolian fault? *Terranova* **14**, 80–86.
- Armijo, R., N. Pondard, B. Meyer, G. Üçarcus, B. Mercier de Lépinay, J. Malavieille, S. Dominguez, M.-A. Gustcher, S. Schmidt, C. Beck, N. Çağatay, Z. Cakir, C. Imren, K. Eris, B. Natalin, S. Özalaybey, L. Tolun, I. Lefèvre, L. Seeber, L. Gasperini, C. Rangin, Ö. Emre, and K. Sarikavak (2005). Submarine fault scarps in the Sea of Mar-

- mara pull-apart (North Anatolian Fault): Implications for seismic hazard in Istanbul, *Geochem. Geophys. Geosyst.* **6**, no. 6, 1–29.
- Atakan, K., A. Ojeda, M. Meghraoui, A. A. Barka, M. Erdik, and A. Bodare (2002). Seismic hazard in Istanbul following the 17 August 1999 Izmit and 12 November 1999 Düzce earthquakes, *Bull. Seismol. Soc. Am.* **92**, no. 1, 466–482.
- Barka, A. (1992). The North Anatolian fault zone, *Annales Tectonicae* **6**, 164–195.
- Barka, A., and K. Kadinsky-Cade (1988). Strike-slip fault geometry in Turkey and its influence on earthquake activity, *Tectonics* **7**, no. 3, 663–684.
- Bender, B. (1983). Maximum likelihood estimation of b values for magnitude grouped data, *Bull. Seismol. Soc. Am.* **73**, 831–851.
- Boore, D. M., and G. Atkinson (2008). Ground motion prediction equations for the average horizontal component of PGA, PGV, and 5%-damped PSA at spectral periods between 0.01 s and 10.0 s, *Earthq. Spectra* **24**, no. 1, 99–138.
- Boore, D. M., W. B. Joyner, and T. E. Fumal (1997). Equations for estimating horizontal response spectra and peak acceleration from western North American earthquakes: A summary of recent work, *Seism. Res. Lett.* **68**, no. 1, 128–153.
- Campbell, K., and Y. Bozorgnia (2008). NGA ground motion model for the geometric mean horizontal component of PGA, PGV, PGD and 5% damped linear elastic response spectra for periods ranging from 0.01 s to 10 s, *Earthquake Spectra* **24**, no. 1, 139–171.
- Chiou, B., and R. Youngs (2008). An NGA model for the average horizontal component of peak ground motion and response spectra, *Earthq. Spectra* **24**, no. 1, 173–215.
- Crowley, H., and J. J. Bommer (2006). Modeling seismic hazard in earthquake loss models with spatially distributed exposure, *Bull. Eq. Eng.* **4**, 249–273.
- Erdik, M., M. Demircioğlu, K. Şeşetyan, E. Durukal, and B. Siyahi (2004). Earthquake hazard in Marmara region, Turkey, *Soil Dyn. Earthq. Eng.* **24**, 605–631.
- Frankel, A. (1995). Mapping seismic hazard in the Central and Eastern United States, *Seism. Res. Lett.* **66**, no. 4, 8–21.
- Gardner, J. K., and L. Knopoff (1974). Is the sequence of earthquakes in southern California, with aftershocks removed, Poissonian? *Bull. Seismol. Soc. Am.* **64**, 1363–1367.
- Gülkan, P., and E. Kalkan (2002). Attenuation modeling of recent earthquakes in Turkey, *J. Seism.* **6**, no. 3, 397–409.
- Gülkan, P., A. Koçyiğit, M. S. Yücemem, V. Doyuran, and N. Başöz (1993). A seismic zones map of Turkey derived from recent data, Middle East Technical University, *Earthquake Engineering Research Center Report No. 93-01*, (in Turkish).
- Hanks, T. C., and H. Kanamori (1979). A moment magnitude scale, *J. Geophys. Res.* **84**, 2348–2350.
- Herrmann, R. B. (1977). Recurrence Relations, *Earthquake Notes* **88**, 47–49.
- Hubert-Ferrari, A., A. A. Barka, E. Jacquess, S. S. Nalbant, B. Meyer, R. Armijo, P. Tapponier, and G. C. P. King (2000). Seismic hazard in the Marmara Sea following the Izmit earthquake, *Nature* **404**, 269–272.
- International Conference of Building Officials (ICBO) (2006). International Building Code, Whittier, CA.
- Kafka, A. L. (2002). Statistical analysis of the hypothesis that seismicity delineates areas where future large earthquakes are likely to occur in the central and eastern United States, *Seism. Res. Lett.* **73**, no. 6, 992–1003.
- Kafka, A. L., and J. R. Walcott (1998). How well does the spatial distribution of smaller earthquakes forecast the locations of larger earthquakes in the northwestern United States? *Seism. Res. Lett.* **69**, 428–440.
- Kalkan, E., and P. Gülkan (2004). Site-dependent spectra derived from ground motion records in Turkey, *Earthq. Spectra* **20**, no. 4, 1111–1138.
- Ketin, I. (1969). Über die nordanatolische Horizontalverschiebung, *Bull. Min. Res. Explor. Inst. Turkey* **72**, 1–28.
- Le Pichon, X., A. M. C. Sengor, E. Demirbag, C. Rangin, C. Imren, R. Armijo, N. Gorur, N. Cagatay, B. Mercier de Lepinay, B. Meyer, R. Saatcilar, and B. Tok (2001). The active main Marmara fault, *Earth Planet. Sci. Lett.* **192**, 595–616.
- Le Pichon, X., N. Chamot-Rooke, C. Rangin, and A. M. C. Sengor (2003). The North Anatolian Fault in the Marmara Sea 2003, *J. Geophys. Res. B Solid Earth Planets* **108**, 2170–2179.
- McClusky, S. 27 coauthors (2000). Global Positioning System constraints on plate kinematics and dynamics in the eastern Mediterranean and Caucasus, *J. Geophys. Res.* **105**, 5695–5719.
- Ministry of Public Works and Settlement (2007). Turkish Seismic Code, Specification for Structures to be Built in Disaster Areas, Ankara, Turkey.
- Motagh, M., J. Hoffmann, B. Kampes, M. Baes, and J. Zschau (2007). Strain accumulation across the Gazikoy—Saros segment of the North Anatolian Fault inferred from Persistent Scatterer Interferometry and GPS measurements, *Earth Planet Sci. Lett.* **255**, no. 30, 432–444.
- Okay, A. I., A. K. Ozcan, C. Imren, A. B. Guney, E. Demirbag, and I. Kuscü (2000). Active faults and evolving strike-slip basins in the Marmara Sea, northwest Turkey: A multichannel seismic reflection study, *Tectonophysics* **321**, 189–218.
- Papazachos, B. C., and C. Papazachou (1997). The Earthquakes of Greece, ZITI Ed., *Thessaloniki* 304 p.
- Parke, J. R., T. A. Minshull, and G. Anderson (1999). Active faults in the Marmara Sea, western Turkey, imaged by seismic reflection profiles, *Terra Nova* **11**, 223–227.
- Parsons, T. (2004). Recalculated probability of  $M \geq 7$  earthquakes beneath the Marmara Sea, Turkey, *J. Geophys. Res.* **109**, B05304, 1–21.
- Parsons, T., S. Toda, R. S. Stein, A. Barka, and J. H. Dieterich (2000). Heightened odds of large earthquake near Istanbul: An interaction-based probability calculation, *Science* **288**, 661–665.
- Petersen, Mark D., Arthur D. Frankel, Stephen C. Harmsen, Charles S. Mueller, Kathleen M. Haller, Russell L. Wheeler, Robert L. Wesson, Yuehua Zeng, Oliver S. Boyd, David M. Perkins, Nicolas Luco, H. Field Edward, Chris J. Wills, and S. Rukstales Kenneth (2008). Documentation for the 2008 Update of the United States National Seismic Hazard Maps, *U.S. Geol. Surv. Open-File Rept. 2008-1128*, 61 p.
- Petersen, M. D., T. R. Topozada, T. Cao, C. H. Cramer, M. S. Reichle, and W. A. Bryant (2000). Active fault near-source zones within and bordering the State of California for the 1997 Uniform Building Code, *Earthq. Spectra* **16**, no. 1, 69–83.
- Pulido, N., A. Ojeda, K. Atakan, and T. Kubo (2004). Strong ground motion estimation in the Marmara Sea region (Turkey) based on scenario earthquake, *Tectonophysics* **39**, 357–374.
- Saroglu, F., O. Emre, and I. Kuscü (1992). Active fault map of Turkey, Maden Tetkik ve Arama (in Turkish).
- Schwartz, D. P., and K. J. Coppersmith (1984). Fault behavior and characteristic earthquakes: Examples from the Wasatch and San Andreas fault zones, *J. Geophys. Res.* **89**, no. B7, 5681–5698.
- Seeber, L., O. Emre, M. H. Cormier, C. C. Sorlien, C. M. G. McHugh, A. Polonia, N. Ozer, N. Cagatay, and The team of the 2000 R/V Urania Cruise in the Marmara Sea (2004). Uplift and subsidence from oblique slip: The Ganos Marmara bend of the North Anatolian Transform, western Turkey, *Tectonophysics* **391**, no. 1–4, 239–258.
- Smith, A. D., T. Taymaz, F. Oktay, H. Yuce, B. Alpar, H. Basaran, J. A. Jackson, S. Kara, and M. Simsek (1995). High-resolution seismic profiling in the Marmara Sea (Northwest Turkey); Late Quaternary sedimentation and sea-level changes, *Spec. Pap. Geol. Soc. Am.* **107**, 923–936.
- Stafford, P. J., F. O. Strasser, and J. J. Bommer (2008). An evaluation of the applicability of the NGA models to ground motion prediction in the Euro-Mediterranean region, *Bull. Earthquake Eng.* **6**, no. 2, 149–177.
- Stein, R. S., A. A. Barka, and J. H. Dieterich (1997). Progressive failure on North Anatolian Fault since 1939 by earthquake stress triggering, *Geophys. J. Int.* **128**, 594–604.

- Straub, C., H-G. Kahle, and C. Schindler (1997). GPS and geologic estimates of the tectonic activity in the Marmara Sea region, NW Anatolia, *J. Geophys. Res.* **102**, no. 27, 587–601.
- Ulusay, R., E. Tuncay, H. Sonmez, and C. Gokceoglu (2004). An attenuation relationship based on Turkish strong-motion data and iso-acceleration map of Turkey, *Eng. Geol.* **74**, no. 3–4, 265–291.
- Weichert, D. H. (1980). Estimation of earthquake recurrence parameters for unequal observation periods for different magnitudes, *Bull. Seismol. Soc. Am.* **70**, 1337–1356.
- Wells, D. L., and K. J. Coppersmith (1994). New empirical relationships among magnitude, rupture length, rupture width, rupture area, and surface displacement, *Bull. Seismol. Soc. Am.* **84**, no. 4, 974–1002.
- Yaltirak, C. (2002). Tectonic evolution of the Marmara Sea and its surroundings, *Mar. Geol.* **190**, 493–529.
- Yenier, E., O. Erdoğan, and S. Akkar (2008). Empirical Relationships for Magnitude and Source-To-Site Distance Conversions using Recently Compiled Turkish Strong-Ground motion Database, *The Fourteenth World Conference on Earthquake Engineering*, October 12–17 2008, Beijing, China.
- Youngs, R. R., and K. J. Coppersmith (1985). Implications of fault slip rates and earthquake recurrence models to probabilistic seismic hazard estimates, *Bull. Seismol. Soc. Am.* **75**, no. 4, 939–964.

U.S. Geological Survey  
Western Region Earthquake Hazards Team  
MS977, 345 Middlefield Rd.  
Menlo Park, California 94025  
ekalkan@usgs.gov

Manuscript received 1 November 2007